ACS Catalysis

Research Article

pubs.acs.org/acscatalysis

Electro- and Photochemical Water Oxidation on Ligand-free Co_3O_4 Nanoparticles with Tunable Sizes

Marek Grzelczak,*[,†,‡,§] Jinshui Zhang,[∥] Johannes Pfrommer,[⊥] Jürgen Hartmann,[†] Matthias Driess,[⊥] Markus Antonietti,[†] and Xinchen Wang*[,∥]

[†]International Joint Laboratory, Department of Colloid Chemistry, Max Planck Institute of Colloids and Interfaces, Research Campus Golm, 14424 Potsdam, Germany

[‡]CIC biomaGUNE, Paseo de Miramón 182, 20009 San Sebastián, Spain

[§]Ikerbasque, Basque Foundation for Science, 48011 Bilbao, Spain

[∥]State Key Laboratory Breeding Base of Photocatalysis, Department of Chemistry, Fuzhou University, Fuzhou, 350002, P. R. China

[⊥]Institute of Chemistry, Technical University Berlin, Strasse des 17. Juni 135, 10623 Berlin, Germany

Supporting Information

ABSTRACT: Splitting of water to hydrogen and oxygen on colloidal catalysts is a promising method for future energy and chemistry cycles. The currently used high-performance oxides containing expensive elements (Ru, Ir) are progressively being replaced by more sustainable ones, such as Co_3O_4. Although the size of the nanoparticles determines their catalytic performance, the control over the particles' diameter is often synthetically difficult to achieve. An additional obstacle is the presence of stabilizing agent, an organic molecule that blocks accessible surface-active centers. Herein, we present how precise control over size of the cobalt oxide nanoparticles (Co_3O_4 NPs), their colloidal stability, and the ligand-free surface affect overall performance of the photocatalytic oxygen evolution. We accordingly correlated the photochemical results with the electrochemical studies, concluding that accessibility of the active species on the particles' surface is crucial parameter in water oxidation.

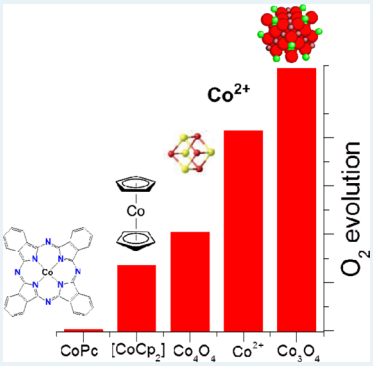

KEYWORDS: *water oxidation, photocatalysis, nanoparticles, cobalt oxide, size control*

1. INTRODUCTION

Water is poised to become the fuel of tomorrow's world if it can be split into molecular oxygen and hydrogen in a sustainable manner, for example, by using abundant solar radiation to drive the reaction.[1−7] As a thermodynamically stable molecule, water requires strong energy input to accomplish overall water splitting, even without considering kinetic barriers for water oxidation and reduction. Currently, the water oxidation process is considered a key bottleneck in actual research development.[8] The difficulty of the water oxidation reaction lies in the relatively high overpotential for the transfer of at least one of four electrons (1.23 eV on average each) accompanied by formation of the oxygen−oxygen bond, which can be minimized by applying a catalyst. The catalyst should exhibit higher chemical stability than water molecules and promote the extraction of $4e^-$ in a concerted manner, thus avoiding charge built up in the strongly oxidizing conditions.

While there is agreement in the classification between homogeneous and heterogeneous catalysts, the chemical stability under photocatalytic action of the former class remains a subject of discussion. For instance, metal complexes (homogeneous catalyst) can decompose during photocatalytic processes to produce nanocrystals, which account for the catalytic activity of the studied material.[9−11] This spontaneous transition from homogeneous to heterogeneous catalyst leads to poor control over the size of newly formed particles, which often result in precipitation and inhibition of the desired chemical pathway. Therefore, ex situ synthesis of a colloidal catalyst with well-controllable size and surface properties allows tuning the catalytic performance. However, to exclude undesired combustion of the ligands under the oxidative conditions, heterogeneous catalysts require a ligand-free surface with maximal surface area that from the synthetic point of view remains a challenging task.

Among a variety of catalysts, spinel-type cobalt oxide has received considerable attention in both electrochemical[12−18] and photochemical[19−21] studies on catalytic water oxidation. Consistently, in both approaches the catalytic performance of the Co_3O_4 was associated with the presence of Co^{3+} species and oxygen vacancies on the surface. Thus, minimization of the particles' size enhances surface activity of the catalyst. The small diameter of the nanoparticles (NPs) additionally augments the number of the surface defects, which improve the binding ability of water molecules. Recently, we have reported sub-5 nm

Received: July 31, 2012
Revised: January 25, 2013
Published: January 29, 2013

spinel-type Co_3O_4 NPs that are suitable building blocks for organic/inorganic heterogeneous photocatalysts.[22] The combination of oxide particles with a conjugated polymer (graphitic carbon nitride) allowed considerable improvement of the water oxidation under visible light. To the best of our knowledge, no effort has been made toward photocatalytic water oxidation in the presence of differently sized NPs.

Here we show that the size of ex situ synthesized Co_3O_4 NPs dramatically affects the yield of photochemical water oxidation. Moreover, our ligand-free Co_3O_4 NPs resulted in an advantageous catalyst in the front of other organometallic complexes containing cobalt ions. In addition, we evaluated electro- and photochemical water oxidation as a function of particles size.

2. EXPERIMENTAL METHODS

2.1. Materials. Cobalt(II) acetate tetrahydrate ($Co(CH_3COO)_2{\cdot}4H_2O$), Cobalt(II) nitrate hexahydrate ($Co(NO_3)_2{\cdot}6H_2O$), sodium hydroxide (NaOH), sodium nitrate ($NaNO_3$), and ammonia (NH_3) 33 wt % were purchased from Sigma-Aldrich. Powdered cobalt oxide (Co_3O_4) and cobalt(II) phtalocyanine were purchased from Alfa Aesar. Mesoporous silica (SBA-15, 550 $m^2\ g^{-1}$)[23] and cubane-like Co_4O_4[24] were synthesized according to previous reports. All solvents used, were of analytic grade.

2.2. Synthesis of 3 nm Cobalt Oxide. Cobalt(II) acetate tetrahydrate ($Co(CH_3COO)_2{\cdot}4H_2O$) (0.5 g) was dissolved in water (2 mL) followed by addition of ethanol (23 mL) under magnetic stirring at 45 °C. After ∼10 min, ammonia was dropwise added (2.5 mL, 33%) under magnetic stirring at 45 °C. Formation of the cobalt oxide NPs takes place at 80 °C, during 3 h. To wash NPs, acetone (100 mL) was added into 27 mL of cobalt oxide crude product, and the solution immediately became turbid. After centrifugation at 4500 rpm for 20 min, the precipitate of Co_3O_4 NPs was obtained, and reddish supernatant containing unreacted cobalt salt was discarded. In the second step of washing, acetone (120 mL) was added into a Co_3O_4 NPs' solution (12 mL in methanol), followed by centrifugation (4500 rpm, 20 min). The remaining NPs were redispersed in methanol (20 mL). The final product of cobalt oxide NPs (120 mg) was obtained by complete evaporation of methanol.

2.3. Synthesis of 10 nm Cobalt Oxide. Cobalt oxide particles with 10 nm diameter were prepared according to the previously reported receipt.[24] Cobalt(II) acetate tetrahydrate ($Co(CH_3COO)_2{\cdot}4H_2O$) (0.5 g) was dissolved in water (2 mL) followed by addition of ethanol (23 mL) under magnetic stirring at 45 °C. After ∼10 min, ammonia was dropwise added (2.5 mL, 33%) under magnetic stirring at 45 °C. Suspension (24 mL) was transferred into Teflon autoclave (48 mL). Formation of the cobalt oxide NPs took place at 150 °C, during 3 h. To wash NPs, acetone (100 mL) was added into 24 mL of crude product, and the solution immediately became turbid. After centrifugation at 4000 rpm for 20 min, the precipitate of Co_3O_4 NPs was obtained. In the second step of washing, acetone (120 mL) was added into Co_3O_4 NPs solution (12 mL in methanol), followed by centrifugation (4000 rpm, 20 min). Remaining NPs were redispersed in methanol (20 mL). Final product of cobalt oxide NPs was obtained by complete evaporation of methanol.

2.4. Synthesis of 40 nm Cobalt Oxide. Cobalt oxide particles with 40 nm of diameter were prepared according to the previously reported recipe.[25] In a typical synthesis, sodium hydroxide (NaOH, 1.2 g) was dissolved in deionized water (100 mL) followed by addition of sodium nitrate ($NaNO_3$) (90 g). The resulting mixture was heated at 105 °C. After 30 min of constant magnetic stirring, cobalt(II) nitrate hexahydrate ($Co(NO_3)_2{\cdot}6H_2O$) (20.0 mL of 1.0 M) was added dropwise within 1 min. The flask with the blue slurry was kept stirring at 105 °C for 43 h. Particles were washed by centrifugation: three times in HCl (50 mL, 2M, 4000 rpm, 20 min); twice in EtOH (100 mL, 4000 rpm, 20 min); twice in tetrahydrofuran (THF, 100 mL, 4000 rpm, 20 min). After the last washing, particles were redispersed in EtOH (200 mL). The final product of cobalt oxide NPs was obtained by complete evaporation of the solvent.

2.5. Impregnation of Mesoporous Silica (SBA-15) with Cocatalysts. SBA-15-cocatalyst composites were prepared by the wet impregnation method. A typical SBA-15/Co_3O_4 with 1.25 wt % Co_3O_4 synthesis is described as follows: Co_3O_4 NPs (5 mg) were dispersed in 15 mL of methanol, followed by addition of as-prepared SBA-15 (550 $m^2\ g^{-1}$) powder (400 mg). After 30 min of ultrasonic treatment, the mixture was transferred to an oil bath (60 °C) to remove the solvent. The resulting powder was further treated at 60 °C in a vacuum oven overnight. This procedure was applied for the impregnation of SBA-15 with another catalyst but using different solvents: Co(II)-water, CoPc-methanol, $CoCp_2$ and Co_4O_4-acetonitrile. The amount of cobalt species was kept constant (5 mg).

2.6. Characterization. Powder X-ray diffraction (XRD) measurements were performed on a Bruker D8 Advance diffractometer with Cu Kα1 radiation (λ = 1.5406 Å). The UV−vis absorption spectra were obtained on a Uvikon 931 with 1 cm optical length. Nitrogen adsorption−desorption isotherms were collected at 77 K using a Micromeritics ASAP 2020 Surface Area and Porosity Analyzer. Transmission electron microscopy (TEM) images were obtained with a ZEISS EM 912Ω instrument at the accelerating voltage of 120 kV.

2.7. Electrochemical Measurements. Electrochemical data were recorded on a Gamry Instruments model Reference 3000 computer controlled potentiostat. All measurements were performed in a one compartment cell using a standard three electrode configuration. Catalytic runs were collected in 0.1 M KPi (measured as pH 7.0) and referenced to a Ag/AgCl reference electrode (Pine Research Instrumentation). Platinum wire served as the auxiliary electrode. Working electrodes composed of a rotating glassy carbon electrode (0.2 cm^2) loaded with Co_3O_4 NPs completed the standard three-electrode configuration. Loadings of Co_3O_4 NPs on the working electrode (0.02 mg/cm^2) were achieved by redispersing 2 mg/mL of Co_3O_4 in MeOH followed by deposition of 10 μL of this solution on the electrode.

2.8. Photocatalytic Measurements. Photocatalytic O_2 production was carried out in a Pyrex top-irradiation reaction vessel connected to a glass closed gas circulation system. For each reaction, the desired amount of cobalt catalyst was dispersed in a 100 mL buffered solution (Na_2SiF_6−$NaHCO_3$, 0.022−0.028 M) with pH held at 5.8. Then 0.975 g of Na_2SO_4, 0.357 g of $Na_2S_2O_8$, and 40 mg of $[Ru(bpy)_3]Cl_2{\cdot}6H_2O$ were added to the reaction solution. The reactant solution was evacuated several times to remove air completely prior to irradiation under a 300 W Xe lamp and a water-cooling filter. The wavelength of the incident light was controlled by using a 455 nm cutoff filter with intensity of 78.2 mW/cm^2 (ILT 950 spectroradiometer). The temperature of the reactant solution was maintained at room temperature by a flow of cooling water

dx.doi.org/10.1021/cs3007523 | ACS Catal. 2013, 3, 383−388

during the reaction. The evolved gases were analyzed by gas chromatography equipped with a thermal conductive detector (TCD) and 5 Å molecular sieve column.[22]

3. RESULTS AND DISCUSSION

We commenced our study with ligand-free cobalt oxide NPs that were synthesized according to recently reported recipes and applying minor modifications.[22,24,26] Diameters of the particles were 3.0 ± 0.6 nm, 9.2 ± 2.6 nm, and 41.7 ± 5.7 nm (Figure 1a–c, d). For simplicity, hereinafter the sizes are

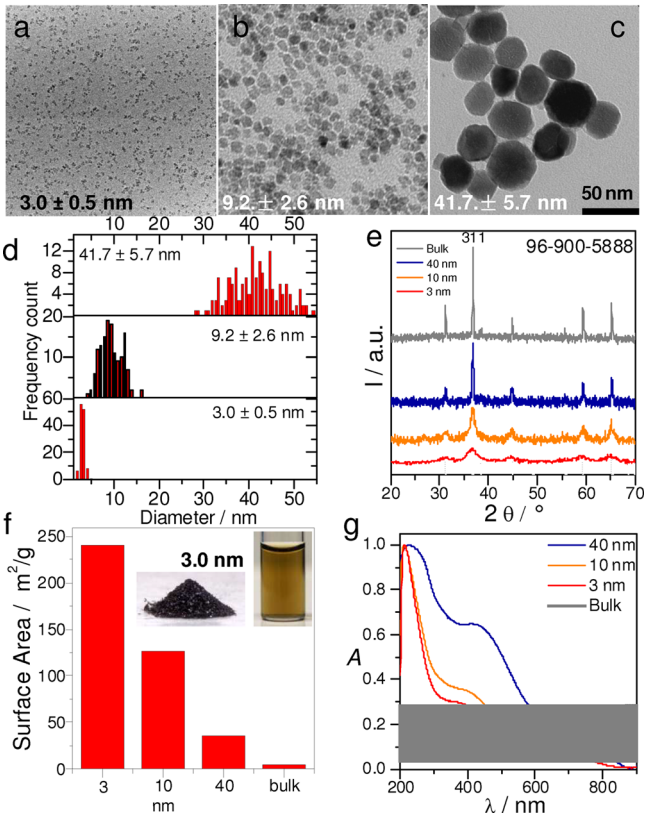

Figure 1. Size evolution of the Co_3O_4 NPs (a–c) TEM images of Co_3O_4 NPs with diameter of 3, 10, and 40 nm and (d) corresponding size distributions. The average diameter was obtained by analysis of over 100 NPs. (e) XRD patterns for particles from images (a–c) with most prominent (311) peaks at 36.7°. All XRD patterns correspond to spinel-like cobalt oxide (card 96-900-5888). (f) Plot of particle diameter versus surface area. Commercial, powdered cobalt oxide (~300 nm) is included for better comparison. Inset: NPs in the form of powder or dispersed in water. (g) UV–vis spectra of colloidal dispersion of Co_3O_4. Characteristic transition bands redshift with increasing particles size. For better comparison, all spectra were normalized at the maximum.

referred to as 3, 10, and 40 nm. Structurally, all particles were exclusively spinel-type cobalt oxide. The XRD patterns consistently showed dominance of the (311) plane for all particles sizes (Figure 1e). Surface area measurements (Brunauer–Emmet–Teller, BET) of the NPs showed a tendency of increasing surface area with decreasing diameter (Figure 1f). The surface area of 3 nm NPs was ~7 times higher than that of 40 nm particles, speaking also for minor aggregation with decreasing particle size. Optical characterization of the Co_3O_4 colloidal dispersion in methanol also confirmed the size-dependent features (Figure 1g). The absorption bands located at 380 and 675 nm for the 3 nm particles correspond to $O^{2-} \rightarrow Co^{2+}$ and $O^{2-} \rightarrow Co^{3+}$, respectively.[27] With increasing particles size, the bands progressively shifted toward higher wavelengths. Thus, the correlation between the size of nanocrystals and the position of absorption bands reminds us of the semiconductor nature of the Co_3O_4 in a similar fashion as do the quantum dots.[28]

Excellent colloidal stability of the Co_3O_4 NPs in water (Figure 1f, inset) stimulated us to study photocatalytic water oxidation directly in the standard homogeneous assay containing ruthenium bipyridine ($Ru[bpy]_3^{2+}$) as a sensitizer, and persulfate as sacrificial agent.[20] For a constant amount of catalyst (5 mg), the amount of evolved oxygen increased with decreasing particle size (Figure 2a). Accordingly, the estimated

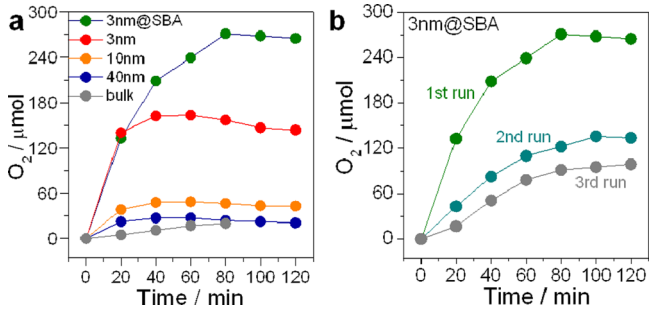

Figure 2. Size-dependent oxygen evolution in aqueous suspension of Co_3O_4 NPs using a $Ru(bpy)_3^{2+}$ visible light sensitization system (λ>450 nm). (a) Time dependent oxygen evolution on Co_3O_4 NPs with different sizes and deposited on the SBA-15 support (green dots). (b) Repetitive use of 3 nm Co_3O_4 on the SBA-15 support.

turnover number (TON) per mole of cobalt progressively increased with decreasing particles sizes; from 0.1 (bulk Co_3O_4) to 2.3 (3 nm Co_3O_4). Thus, this difference leads us to conclude that the surface accessibility of the catalyst is a main factor ruling the catalytic performance.

It is worth noting that after the first 20 min of the reaction, the amount of the evolved oxygen abruptly leveled off to reach a plateau (Figure 2a, red, orange, and blue dots). It is reasonable to assume that constant chemical changes in the reacting solution (e.g., gas evolution, proton gradient) disturb colloid dispersion resulting in gradual flocculation. Thus, the transition from colloidal to suspension phase causes progressive deactivation of the catalyst. TEM analysis of the sample after catalytic reaction confirmed the formation of the aggregates over several micrometers in size (see Supporting Information, Figure S1).

To further prevent aggregation of the colloids during photolysis we anchored 3 nm Co_3O_4 NPs to the surface of mesoporous silica (SBA-15) (hereinafter referred to as 3 nm@SBA), facilitating homogeneous distribution of the reactive centers. The SBA-15 has been recently proposed as a successful template for metal oxide nanocrystals that efficiently catalyzed water oxidation.[20,29] Similar, in the present study, the oxygen evolution was significantly improved for 3 nm@SBA, as compared to freely dispersed 3 nm Co_3O_4 NPs (Figure 2a, green dots). It is worth stressing, that mesoporous silica, apart from preventing particle aggregation, scatters incoming light, thus enhancing light absorbance by the photosensitizer. In addition, tight heterogeneous junctions between the silica template and the nanocrystals can also alter electronic structure of the cobalt. The XPS analysis revealed a shift of the $Co_{2p2/3}$

dx.doi.org/10.1021/cs3007523 | ACS Catal. 2013, 3, 383–388

peak by ~1 eV toward higher binding energy in 3 nm@SBA composites as compared to bulk Co_3O_4. (see Supporting Information, Figure S2). As the shift indicates an increase of cobalt oxidation state, it could similarly affect the overpotential in water oxidation reactions. Our observations, indeed, are in good agreement with the previous studies. The yield of catalytic oxidations of the organic compounds on Co_3O_4/SBA composites has been considerably higher than on the cobalt oxide alone.[30,31]

Depositing particles on the solid substrate allowed us to recover the 3 nm@SBA once the reaction was finished. After the first run, 3 nm@SBA was recovered and reused with another fresh solution for subsequent photocatalytic reaction (Figure 2b). The amount of evolved oxygen during the second run was 50% of initial activity, while the third run resulted in 36% of the initial activity. The lower O_2 yield in the second and third run was due to recovery loss of catalytic particles. Note that the addition of a new portion of $Ru[bpy]_3^{2+}$ into the reactor, after reaching the plateau during first run, failed to recover the initial rate of oxygen evolution. The XRD analysis of the precipitate after the first run revealed a considerable amount of insoluble buffer (Na_2SiF_6) (see Supporting Information, Figures S3 and S4). We speculate that activity loss is due to the temporal passivation of cocatalyst surface by poorly soluble buffer molecules, which are well-known to have short lifetime in a water oxidation reaction. Therefore, a thorough washing process and resuspension in fresh assay solution was mandatory to recover, at least partially, the initial catalytic activity. These experiments showed that 3 nm@SBA can be recycled for further reactions, especially when coupled to a highly oxidation-stable photosensitizer.

Electrochemical analysis confirmed the size dependent catalytic activity of Co_3O_4 NPs. Because of chemical instability in acid medium, spinel-type cobalt oxide NPs have been mostly studied at high pH.[16] We extend the electrochemical properties of Co_3O_4 NPs to neutral pH. Size dependent electrochemical studies were carried out on the 3, 10, and 40 nm Co_3O_4 NPs (no SBA-15). As a control, we used bulk Co_3O_4 with an approximately 300 nm diameter. Cyclic voltammetry of the glassy carbon anode with bulk Co_3O_4 in the 0.1 M potassium phosphate (pH 7) showed low catalytic activity (Figure 3a, gray line). In the presence of the Co_3O_4 NPs the magnitude of the current density at constant particle loading (0.02 mg/cm^2) progressively increases with decreasing particles size, as the number of the available active species increases. All CV scans reveal features typical for cobalt oxide located at potentials lower than the catalytic waves, which correlates to the $Co^{2+} \rightarrow Co^{3+}$ and $Co^{3+} \rightarrow Co^{4+}$ redox steps.[32,33] Recently, other groups have suggested that spinel-type cobalt oxide under oxidative conditions is reversibly remodeled into oxide layers containing Co(IV).[32−35] Following this argument, it is reasonable to expect that particles presented here follow a similar reversible chemical transition at potentials lower than the catalytic wave. However, above the catalytic wave there is an abrupt onset of the catalytic current at 1.45 V that is due to water oxidation (Figure 3). For the smallest Co_3O_4 NPs (3 nm), we estimated the overpotential for water oxidation, that is, 660 mV at 1 mA/cm^2. In the context of available cobalt catalysts, our spinel-type cobalt oxide exhibits overpotential of ~250 mV higher than the CoPi catalyst proposed by Kanan and Nocera.[36] Beside lower catalytic performance of Co_3O_4, it facile manipulation and storage allows for fast implementation into a desired catalytic environment. In fact, we have recently showed that Co_3O_4 NPs could be easily combined with the polymeric photocatalyst.[22]

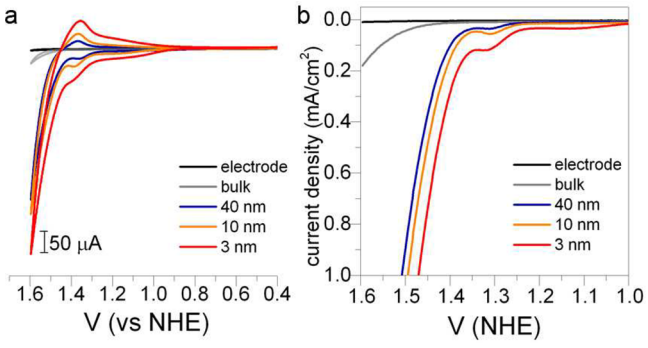

Figure 3. Electrochemical characterization of the Co_3O_4 NPs. (a) Size-dependent cycling voltammograms and (b) polarization activity of NPs in 0.1 M KPi electrolyte at pH 7. Potential recorded using 0.2 cm^2 glassy carbon working electrode with catalyst loading of 0.02 mg/cm^2. All potential were measured against a Ag/AgCl reference at 2 mV/s and converted to NHE potential by using E(NHE) = E(Ag/AgCl) + 0.198 V.

Although, cobalt-based compounds have attracted much attention for water oxidation reaction, their comparison in terms of their catalytic activity, based on literature data, is rather difficult. Thus, to highlight the importance of ligand-free nanoclusters in water oxidation, we compared Co_3O_4 with a series of cobalt-based molecular compounds. To maximize structural diversity between the compounds we choose mononuclear cobalt complex (cobalt(II) phthalocyanine (CoPc) and cobaltocene ($CoCp_2$)), tetranuclear complex (di-pyridyldiolato-acetato coordinated cubane-like cluster cation, $\{Co_4[(C_5H_4N)_2C(OH)O]_4(O_2CMe)_3(H_2O)\}$ (Co_4O_4)), and finally $Co(NO_3)_2$ possessing no organic ligand. (Figure 4).[33] To optimize the photocatalytic reactions for each compound, we used a standard homogeneous assay containing ruthenium complex as photocatalyst. In addition, the issues with partial insolubility/aggregation were overcome by impregnation of all samples onto SBA-15 (see experimental part).

The CoPc has been recently reported to be a good catalyst for water oxidation in the presence of an n-type organic semiconductor, but it required an external bias of 0.4 V.[37] Under conditions presented here, the activity of CoPc is rather negligible (Figure 4), which indicates inhibition of Co−OH_2 formation by the strong Co-ligand interactions. Next, we used cobaltocene that structurally contains less rigidly coordinated cobalt ions as compared to the CoPc (Figure 4). Although $CoCp_2$ exhibit better catalytic behavior than phthalocyanine, its performance is much lower than observed for 3 nm@SBA (Figure 4). It has been shown that the Cp ligand in the mononuclear complexes containing cobalt[11] or iridium[38] can undergo oxidation to form acetic and formic acids. The metal center, however, dissociates to nanoparticulate aggregates consisting of $Co(OH)_x$ with diameter above 100 nm. Thus, a similar ligand oxidation may occur in the present study, leading to the growth of hydroxide, which facilitates formation of chemical bonds between cobalt and water. A tetranuclear cubane-like Co_4O_4 cluster cation with dipyridyldiolato and acetate ligands was investigated as a further example,[39,40] showing improvement of oxygen evolution that is in good agreement with the previous reports.[41] Notwithstanding, the yield of O_2 evolution for Co_4O_4 is almost half the yield observed for 3 nm@SBA. The limited accessibility of water

dx.doi.org/10.1021/cs3007523 | ACS Catal. 2013, 3, 383−388

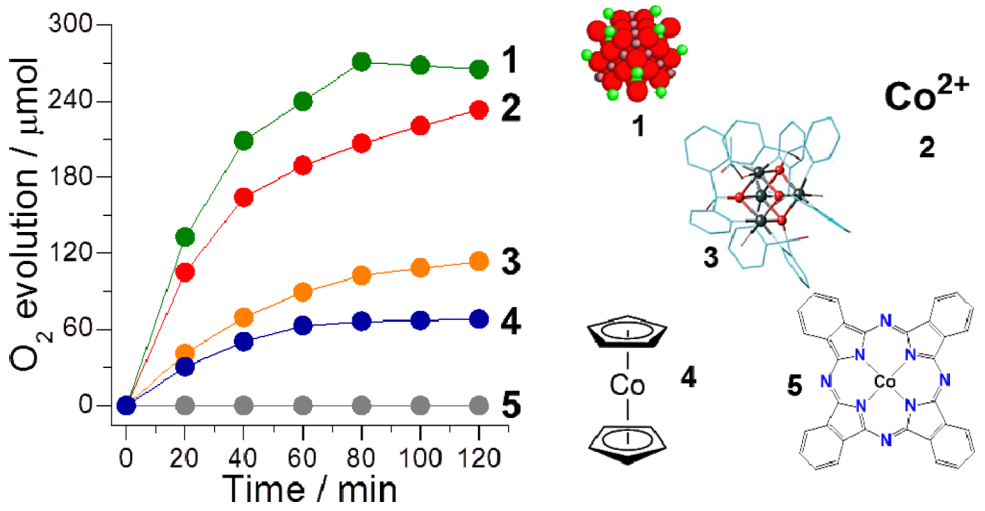

Figure 4. Visible light-induced oxygen evolution from a variety of cobalt compounds deposited on SBA-15. Ligand-free Co_3O_4 NPs showed superior activity toward water oxidation than molecular based cocatalysts.

molecules that is due to the dipyridyldiolato and acetate ligands can alter the redox chemistry of Co ions. Finally, we tested $Co(NO_3)_2$, which also showed lower O_2 evolution than in 3 nm@SBA. The activity of the cobalt nitrate toward water oxidation has been associated with a photoactive binuclear complex[42] and a Co(IV) intermediate,[43] whose formation is promoted by the absence of the competing ligand. Again, it has been shown that $Co(NO_3)_2$ forms cobalt-containing particles that precipitate out of the solution, leading to a gradual decrease of the activity.[44,45] Hong et al. have shown that at longer irradiation time, the size of the particles derived from cobalt nitrate can reach 500 nm.[11] Our results, then, indicate that cobalt complexes, especially $CoCp_2$ and $Co(NO_3)_2$, can act as efficient precatalysts, which are oxidized during the photocatalytic water oxidation to produce a reactive catalyst in the form NPs.[46]

As shown above, decreasing the size of Co_3O_4 NPs increases the catalytic performance of water oxidation. One could expect a similar tendency for in situ formed NPs during photocatalytic reaction from molecular compounds. Spiccia and co-workers have shown that a bioinspired molecular catalyst based on Mn clusters reversibly transforms to manganese oxide NPs with a diameter of 1−2 nm,[9,47] while Grotjahn et al. reported that a number of iridium complexes form iridium oxide NPs with diameter below 10 nm.[48] Thus, the control over the composition and the size of in situ formed particles remains a difficult task. The ex situ synthesis, however, allows for better control over surface accessibility and dimensionality of the catalyst NPs.

4. CONCLUSIONS

In summary, we have shown that the efficiency of electro- and photochemical O_2 evolution depends on available surface area, which increases with decreasing particle size. We are aware that a direct comparison of both processes is rather difficult, since the mechanism ruling both reactions follows different chemical pathways. Especially difficult to analyze is the photochemical water oxidation, in which a ruthenium complex and persulfate can additionally react with water molecules. Notwithstanding, the tendency of increased activity with decreasing particle size, reported in this article, clearly indicates—within the experimental framework—that availability of the surface cobalt atoms is a primary factor ruling water oxidation, independently of the chemical pathway. An additional factor of great importance is the accessibility of the oxide surface to the reacting molecules. We have shown, in comparative water photolysis on the Co_3O_4 and cobalt-based molecular compounds, that a ligand-free surface is crucial for good catalytic efficiency.

■ ASSOCIATED CONTENT

Supporting Information

TEM characterization of the particles after photolysis. XPS spectra of the Co_3O_4 and Co_3O_4@SBA. TEM characterization of the Co_3O_4@SBA before and after photolysis. XRD spectra of the Co_3O_4 before and after photolysis. This material is available free of charge via the Internet at http://pubs.acs.org.

■ AUTHOR INFORMATION

Corresponding Author

*E-mail: grzelczak.marek@gmail.com (M.G.), xcwang@fzu.edu.cn (X.W.).

Notes

The authors declare no competing financial interest.

■ ACKNOWLEDGMENTS

Financially supported by the BMBF ("Light to Hydrogen" (L2H) project), the National Basic Research Program of China (2013CB632405), and the National Natural Science Foundation of China (21033003 and 21173043).

■ REFERENCES

(1) Maeda, K.; Teramura, K.; Lu, D.; Takata, T.; Saito, N.; Inoue, Y.; Domen, K. *Nature* **2006**, *440*, 295.
(2) Chen, X.; Shen, S.; Guo, L.; Mao, S. S. *Chem. Rev.* **2010**, *110*, 6503−6570.
(3) Walter, M. G.; Warren, E. L.; McKone, J. R.; Boettcher, S. W.; Mi, Q.; Santori, E. A.; Lewis, N. S. *Chem. Rev.* **2010**, *110*, 6446−6473.
(4) Kudo, A.; Miseki, Y. *Chem. Soc. Rev.* **2009**, *38*, 253−278.
(5) Cook, T. R.; Dogutan, D. K.; Reece, S. Y.; Surendranath, Y.; Teets, T. S.; Nocera, D. G. *Chem. Rev.* **2010**, *110*, 6474−6502.
(6) Maeda, K.; Domen, K. *J. Phys. Chem. Lett.* **2010**, *1*, 2655−2661.
(7) Reece, S. Y.; Hamel, J. A.; Sung, K.; Jarvi, T. D.; Esswein, A. J.; Pijpers, J. J. H.; Nocera, D. G. *Science* **2011**, *334*, 645−648.

(8) Inoue, H.; Shimada, T.; Kou, Y.; Nabetani, Y.; Masui, D.; Takagi, S.; Tachibana, H. *ChemSusChem* **2011**, *4*, 173−179.
(9) Hocking, R. K.; Brimblecombe, R.; Chang, L.-Y.; Singh, A.; Cheah, M. H.; Glover, C.; Casey, W. H.; Spiccia, L. *Nat. Chem.* **2011**, *3*, 461−466.
(10) Stracke, J. J.; Finke, R. G. *J. Am. Chem. Soc.* **2011**, *133*, 14872−14875.
(11) Hong, D.; Jung, J.; Park, J.; Yamada, Y.; Suenobu, T.; Lee, Y.-M.; Nam, W.; Fukuzumi, S. *Energy Environ. Sci.* **2012**, *5*, 7606−7616.
(12) Iwakura, C.; Honji, A.; Tamura, H. *Electrochim. Acta* **1981**, *26*, 1319−1326.
(13) Rasiyah, P.; Tseung, A. C. C. *J. Electrochem. Soc.* **1983**, *130*, 365−368.
(14) Brossard, L. *J. Appl. Electrochem.* **1991**, *21*, 612−618.
(15) Singh, R. N.; Mishra, D.; Anindita; Sinha, A. S. K.; Singh, A. *Electrochem. Commun.* **2007**, *9*, 1369−1373.
(16) Esswein, A. J.; McMurdo, M. J.; Ross, P. N.; Bell, A. T.; Tilley, T. D. *J. Phys. Chem. C* **2009**, *113*, 15068−15072.
(17) Hamdani, M.; Singh, R. N.; Chartier, P. *Int. J. Electrochem. Sci.* **2010**, *5*, 556−577.
(18) Liang, Y.; Li, Y.; Wang, H.; Zhou, J.; Wang, J.; Regier, T.; Dai, H. *Nat. Mater.* **2011**, *10*, 780−786.
(19) Harriman, A.; Pickering, I. J.; Thomas, J. M.; Christensen, P. A. *J. Chem. Soc., Faraday Trans. 1* **1988**, *84*, 2795−2806.
(20) Jiao, F.; Frei, H. *Angew. Chem., Int. Ed.* **2009**, *48*, 1841−1844.
(21) Kim, Y.-Y.; Meldrum, F. C.; Walsh, D. *Polym. Chem.* **2011**, *2*, 1375−1379.
(22) Zhang, J.; Grzelczak, M.; Hou, Y.; Maeda, K.; Domen, K.; Fu, X.; Antonietti, M.; Wang, X. *Chem. Sci.* **2012**, *3*, 443−446.
(23) Chen, X.; Zhang, J.; Fu, X.; Antonietti, M.; Wang, X. *J. Am. Chem. Soc.* **2009**, *131*, 11658−11659.
(24) Dong, Y.; He, K.; Yin, L.; Zhang, A. *Nanotechnology* **2007**, *18*, 435602.
(25) Feng, J.; Zeng, H. C. *Chem. Mater.* **2003**, *15*, 2829−2835.
(26) Xu, R.; Zeng, H. C. *J. Phys. Chem. B* **2003**, *107*, 926−930.
(27) Pal, J.; Chauhan, P. *Mater. Charact.* **2010**, *61*, 575−579.
(28) Xu, R.; Zeng, H. C. *Langmuir* **2004**, *20*, 9780−9790.
(29) Jiao, F.; Frei, H. *Chem. Commun.* **2010**, *46*, 2920−2922.
(30) Szegedi, Á.; Popova, M.; Minchev, C. *J. Mater. Sci.* **2009**, *44*, 6710−6716.
(31) Hu, L.; Yang, X.; Dang, S. *Appl. Catal., B* **2011**, *102*, 19−26.
(32) Gerken, J. B.; McAlpin, J. G.; Chen, J. Y. C.; Rigsby, M. L.; Casey, W. H.; Britt, R. D.; Stahl, S. S. *J. Am. Chem. Soc.* **2011**, *133*, 14431−14442.
(33) Chou, N. H.; Ross, P. N.; Bell, A. T.; Tilley, T. D. *ChemSusChem* **2011**, *4*, 1566−1569.
(34) Yeo, B. S.; Bell, A. T. *J. Am. Chem. Soc.* **2011**, *133*, 5587−5593.
(35) Dau, H.; Limberg, C.; Reier, T.; Risch, M.; Roggan, S.; Strasser, P. *ChemCatChem* **2010**, *2*, 724−761.
(36) Kanan, M. W.; Nocera, D. G. *Science* **2008**, *321*, 1072−1075.
(37) Abe, T.; Nagai, K.; Kabutomori, S.; Kaneko, M.; Tajiri, A.; Norimatsu, T. *Angew. Chem., Int. Ed.* **2006**, *45*, 2778−2781.
(38) Hetterscheid, D. G. H.; Reek, J. N. H. *Chem. Commun.* **2011**, *47*, 2712−2714.
(39) Polarz, S.; Orlov, A. V.; Van den Berg, M. W. E.; Driess, M. *Angew. Chem., Int. Ed.* **2005**, *44*, 7892−7896.
(40) Ganga, G. L.; Puntoriero, F.; Campagna, S.; Bazzan, I.; Berardi, S.; Bonchio, M.; Sartorel, A.; Natali, M.; Scandola, F. *Faraday Discuss.* **2011**, *155*, 177−190.
(41) McCool, N. S.; Robinson, D. M.; Sheats, J. E.; Dismukes, G. C. *J. Am. Chem. Soc.* **2011**, *133*, 11446−11449.
(42) Anbar, M.; Pecht, I. *J. Am. Chem. Soc.* **1967**, *89*, 2553−2556.
(43) Brunschwig, B. S.; Chou, M. H.; Creutz, C.; Ghosh, P.; Sutin, N. *J. Am. Chem. Soc.* **1983**, *105*, 4832−4833.
(44) Gerasimov, O. V.; Elizarova, G. L.; Parmon, V. N. *J. Photochem. Photobiol., B* **1992**, *13*, 335−338.
(45) Elizarova, G. L.; Zhidomirov, G. M.; Parmon, V. N. *Catal. Today* **2000**, *58*, 71−88.
(46) Limburg, B.; Bouwman, E.; Bonnet, S. *Coord. Chem. Rev.* **2012**, *256*, 1451−1467.
(47) Hocking, R. K.; Chang, S. L. Y.; MacFarlane, D. R.; Spiccia, L. *Aust. J. Chem.* **2012**, *65*, 608−614.
(48) Grotjahn, D. B.; Brown, D. B.; Martin, J. K.; Marelius, D. C.; Abadjian, M.-C.; Tran, H. N.; Kalyuzhny, G.; Vecchio, K. S.; Specht, Z. G.; Cortes-Llamas, S. A.; Miranda-Soto, V.; Van Niekerk, C.; Moore, C. E.; Rheingold, A. L. *J. Am. Chem. Soc.* **2011**, *133*, 19024−19027.